BUILD SIMUL (2023) 16: 1863–1879
https://doi.org/10.1007/s12273-023-1027-z

Design and performance testing of a novel building integrated photovoltaic thermal roofing panel

Mehdi Zadshir[2,3,§], Chunlin Wu[1,2] (✉), Xiaokong Yu[2,§], Huiming Yin[2] (✉)

1. Shanghai Institute of Applied Mathematics and Mechanics, Shanghai Key Laboratory of Mechanics in Energy Engineering, Shanghai Frontier Science Center of Mechanoinformatics, School of Mechanics and Engineering Science, Shanghai University, Shanghai 200072, China

2. Department of Civil Engineering and Engineering Mechanics, Columbia University, 610 Seeley W. Mudd 500 West 120th Street, New York, NY 10027, USA

3. PVT Clean Energy LLC, 7 Industry Street #5, Poughkeepsie, NY 12603, USA

Abstract

A novel building integrated photovoltaic thermal (BIPVT) roofing panel has been designed considering both solar energy harvesting efficiency and thermal performance. The thermal system reduces the operating temperature of the cells by means of a hydronic loop integrated into the backside of the panel, thus resulting in maintaining the efficiency of the solar panels at their feasible peak while also harvesting the generated heat for use in the building. The performance of the proposed system has been evaluated using physical experiments by conducting case studies to investigate the energy harvesting efficiency, thermal performance of the panel, and temperature differences of inlet/outlet working liquid with various liquid flow rates. The physical experiments have been simulated by coupling the finite element method (FEM) and finite volume method (FVM) for heat and mass transfer in the operation. Results show that the thermal system successfully reduced the surface temperature of the solar module from 88 °C to as low as 55 °C. Accordingly, the output power that has been decreased from 14.89 W to 10.69 W can be restored by 30.2% to achieve 13.92 W. On the other hand, the outlet water from this hydronic system reaches 45.4 °C which can be used to partially heat domestic water use. Overall, this system provides a versatile framework for the design and optimization of the BIPVT systems.

Keywords

building integrated photovoltaic thermal panels
conjugate heat transfer
energy harvesting efficiency
solar panels
hydronic system

Article History

Received: 15 February 2023
Revised: 20 March 2023
Accepted: 02 April 2023

1 Introduction

The increasing energy demand and the depleting fossil fuel reserves have urged governments to look for more renewable and eco-friendly energy resource alternatives. Solar energy is an abundant source of energy, and with newer technologies in the semiconductor industry, applications of silicon solar cells have grown substantially since their invention in 1954 at Bell Labs (Fraas 2014; Ghosh 2017). Among different solar cell technologies, polycrystalline silicon accounts for more than 91% of the market share (Ananthachar 2008). In silicon solar cells, the high energy photons excite the electrons and form a current inside the cell (De la Torre et al. 2006; Ushasree and Bora 2019), while the weak photons turn into heat and increase the surface temperature of the cell up to 80 °C (De la Torre et al. 2006). Increased temperature has an adverse effect on the efficiency of the solar panel. Mainly, the open-circuit voltage of the cell decreases with the temperature increase (Figure 1) (Fthenakis and Lynn 2018). This results in less output power and thus, decreases the efficiency of the panel. Under Standard Test Conditions (STC), for every degree of rise in temperature, the efficiency decreases by about 0.40%–0.50% (Natarajan et al. 2011). In addition, the absorbed heat accelerates the aging of the solar cells and shortens their lifespan. Therefore, efforts to address this issue and lower the surface temperature

E-mail: chunlinwu@shu.edu.cn (Chunlin Wu); yin@civil.columbia.edu (Huiming Yin)

§ Mehdi Zadshir and Xiaokong Yu contributed equally to this work.

List of symbols

D	diameter of the tube	t	time (min)
L	characteristic length of the tube	u	flow speed
Q	quantum of the flow meter	ν	kinematic viscosity
Re	Reynolds number		

of the operating solar panels are important to achieve the maximum gain from the solar cells.

Researchers have found that it is possible to reduce the surface temperature of a solar panel and thus, maintain its efficiency at the optimal level (Chen and Yin 2016). On the other hand, this extracted heat can be put into use for other applications such as domestic water heating or partial air conditioning in cold climates. The idea of combining these two has been a motivation for many researchers. Yet, the limiting factor is to find a method or material to benefit from the wide range of the solar spectrum. However, considering the fact that silicon photovoltaic solar cells, which are more common and available in the market, absorb the infrared wavelength of the sunshine, a less complex way to combine both solar photovoltaic (PV) and thermal is to indirectly harness the heat that is generated in the modules.

Yang and Yin (2011) introduced a novel idea by using a thermoelectric (TE) module for thermal energy harvesting. In this multilayer design, a semiconductor material, bismuth telluride (Bi_2TE_3), is used as a TE generator layer underneath the PV cells, and then a back layer of functionally graded material (FGM) with cast water tubes made of copper is implemented. The novelty of the design was the application of the FGM layer, in which the thermal resistance gradually changes with depth (Zhang et al. 2020). The heat from the solar panels is first transferred to the thermoelectric layer to generate electricity and then dissipated to the water that flows in the copper tubes embedded in the FGM material.

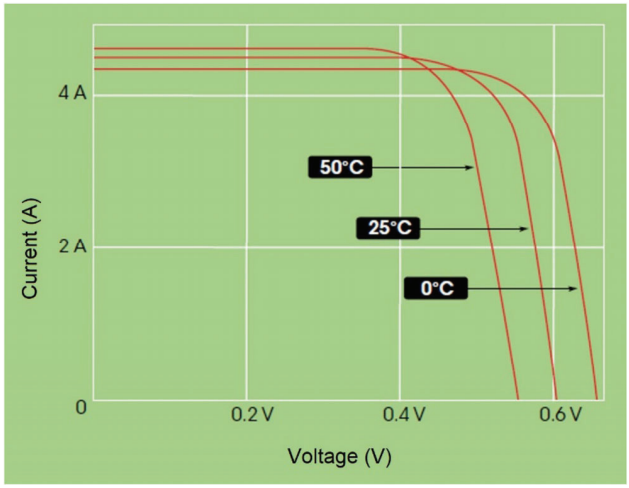

Fig. 1 Effect of temperature on the I-V Curve (Fthenakis and Lynn 2018; reprinted with permission ©2018 John Wiley & Sons)

In a similar work from the same group, experiments on the hybrid solar panel with PV cells and FGM layer with water tubes showed that the system can lower the temperature of the solar panel from 55 °C to 32 °C at 1100 W/m^2 irradiation (Yang et al. 2012). The authors used a finite element model (FEM) simulation for the thermal performance of their panel. However, the temperature distribution of the working fluid was simplified as a linear function of the path and the forced convection as a Nusselt number related quantity obtained by Bejan (2013). The improved version of the panel included the highly thermal conductive aluminum layer on the top with the thermally insulated high-density polyethylene (HDPE) at the bottom of the FGM (Yin et al. 2013). The designed panel can be used as an integrated part of the roof in the building envelope and thus, can bear structural load due to its rigidity and strength.

One factor to consider in such composite materials is the thermal stress and deformation of each layer due to the thermal mismatch of the layers under environmental conditions, which could affect the physical integrity and therefore, the longevity of the material (Zhang et al. 2021). Examples could be laminated photovoltaic silicon solar panels and novel sun-powered solar blinds (Zhang et al. 2019; Lin et al. 2020). Finally, Chen et al. (2018) further matured this building integrated photovoltaic and thermal (BIPVT) design by performing more tests and showing that at a water flow rate of 150 ml/min and under 1000 W/m^2 solar irradiation, the efficiency is enhanced by 24% compared with the panel with no cooling system.

In another work, Yang et al. (2012) applied the finite element method to study the building integrated photovoltaic (BIPV) system with a substrate of functionally graded materials. To simplify the simulation process of flowing liquid, the authors assumed a linear temperature distribution along the direction of the water tubes, which compromises the accuracy of solutions and can seldom be extended for our current model. Nasrin et al. (2018) applied a FEM model with commercial software COMSOL to investigate a PV system with high irradiation and fluid cooling system, where the liquid is entirely simulated by FEM. The authors comprehensively illustrated the advantage of the

implementation of the cooling system through comparison with a conventional system, and they emphasized the overall efficiency. In addition, other computer software has been used, such as TRANS (Lamnatou et al. 2015) and an artificial neural network (ANN) (Ghani et al. 2012). Salameh et al. (2021) proposed a novel three-dimensional model to simulate a PV/T system in the United Arab Emirates, where only one channel flow is considered. Misha et al. (2020) investigated the thermal performance of the PVT system in Malaysia. Their work combined FEM and the finite volume method (FVM) in ANSYS, where FEM and FVM handle the solids and fluid parts, respectively.

Here in this paper, a new design for the thermal management of photovoltaics (PV) is presented using a hydronic loop system on the backside of the panel. In this design, aluminum tubes that are cast inside a foamed aluminum layer are integrated into the backside of the solar panel, and water circulates inside tubes in a closed loop. Due to the high conductivity of foamed aluminum, the heat generated during the collection of solar energy can be quickly transferred to the substrate and thus captured by the water in the embedded tubes. The water absorbs the heat when it meets the panel and thus, reduces the surface temperature of the cells and makes them cooler. Therefore, the water acts as both a heat sink and a heat collector. The heated water is then transferred to the facility room of the building via a pump and through contact with a heat exchanger, the heat is transferred to a water tank indirectly. As a result, the temperature of the panel is regulated during the operation time, and the harvested heat could be used for partially warming the water for applications in the building. This system not only maintains the efficiency of the solar panels at their feasible peak but also harvests heat and reduces the total energy consumption of the building. In addition, the strong foamed aluminum layer can be a supporting substrate, thus, making this BIPVT system to be used in the roof structure directly instead of being placed on the roof, which is the common practice for solar panels. To investigate the thermal performance of this solar energy harvesting system, several case studies have been conducted based on trending numerical methods. By doing both simulations and experiments, the hypothesis of a temperature regulation system that can effectively improve the efficiency of the solar panel while also harvesting heat is examined. However, the mechanical testing related to the strength of the building integrated panel is outside the scope of this paper.

2 Concept and design outline

The novel model aims to lower the temperature and improve the efficiency of energy harvesting in a silicon solar module. And this paper is an improvement of the design concept and method of recent work by Chen et al. (2018). The components of this design are shown in Figure 2. A protective layer, which is glass, is placed on top, and an EVA (ethylene vinyl acetate) film is used to sandwich the photovoltaic layer. A foamed aluminum layer with tubes cast inside the layer is integrated into the backside of the solar panel. The tubes are made of aluminum and thus, are highly conductive.

An absorbing fluid with high heat capacity which could be water (in this experiment) or a mixture of water and glycol (for anti-freeze properties) is circulated inside the tubes in a closed loop, while being in contact with a heat exchanger to transfer the heat out of the tubes, resulting in the reduction of the surface temperature of the cells. The heated fluid could then be transferred to the facility room of the building via a pump to indirectly heat a water tank, which could be used for indoor heated water usage. Therefore, the water is acted as both a heat sink and a heat collector. Providing a large surface area for heat exchange while being lightweight, having a relatively high thermal conductivity, resistance to thermal shocks, high pressures, and high temperatures resistance, and the recyclability of the aluminum make it the right choice as the back support to embed this system. The lightweight concrete layer or an alternative foamed aluminum layer (Zadshir and Wu 2019), which encloses the tubes, has open pores that can be filled in the future with phase change materials to absorb and release heat with a time latency. Therefore, the daily temperature fluctuation of the building will significantly be lowered, which per se has a role in the total energy consumption. The foamed aluminum layer is assumed to be homogenous, with a consistent thermal conductivity. A finished prototype of this BIPVT panel is shown in Figure 3.

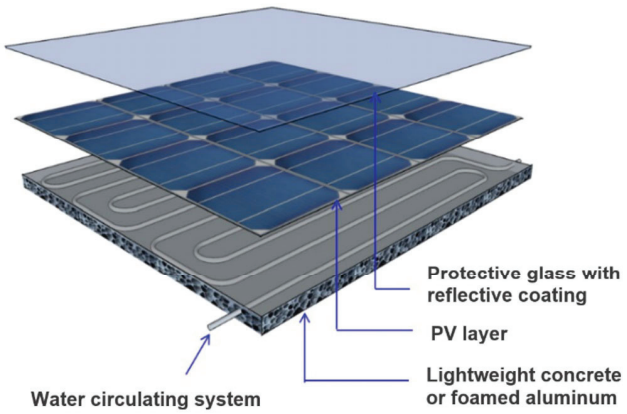

Fig. 2 Schematic illustration of the hydronic system

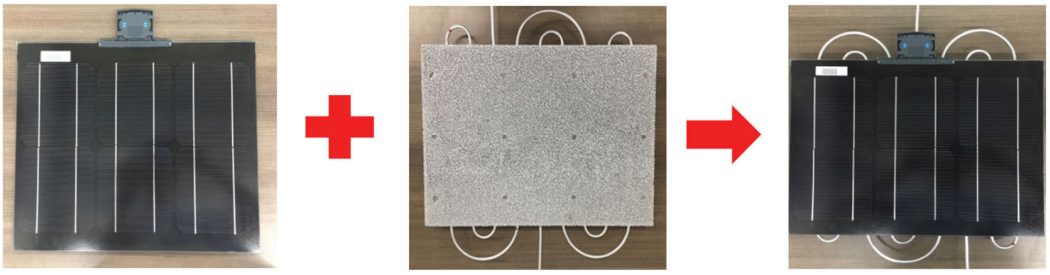

Fig. 3 Assembled BIPVT panel in the lab for testing

3 Performance testing

3.1 Experiment setup

In order to simulate the sunlight on the panel, a solar lamp tester was used, in which the irradiation of the light can be adjusted to mimic the sunlight intensity at different weather conditions and locations.

In general, there are two testing conditions in the solar industry: Photovoltaics for Utility Scale Applications (PVUSA) Test Conditions or more commonly known as PTC, and Standard Test Conditions (STC). Here, the STC test conditions were used with a cell temperature of 25 °C, an irradiance of 1000 W/m^2, and an air mass of 1.5 (AM 1.5).

Considering the reverse correlation between the panel's surface temperature and its output power (efficiency), the experiment was designed in such a way the temperature change over time and the corresponding effect on the power. The procedure for the experiments is shown in Figure 4. First, the data acquisition (DAQ) system is started to make sure the data will be collected before the solar lamp is turned on. After 5 minutes of collecting data when the panel is at room temperature and only exposed to the ambient conditions, we turn on the solar lamp.

Under the STC, different water flow rates of 100, 200, 300, 400, 500, and 600 ml/min were examined and the changes in the I-V curves of the BIPVT panel are measured. Also, the effect of the hydronic system will be compared

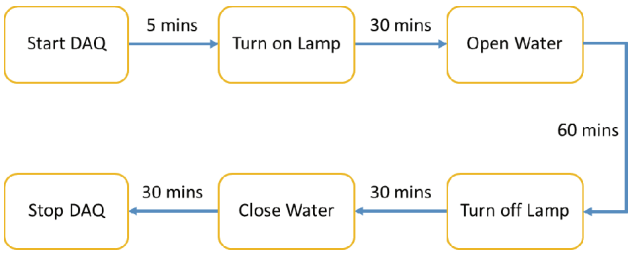

Fig. 4 Flowchart of the procedure for performance testing of the BIPVT panel

with a regular panel without this cooling technology. Another panel with the same cell specifications (I_{sc} = 5.2 A, V_{oc} = 3.7 V, and P_{max}=14 W) and geometry of 40 cm (15.7") by 30 cm (11.8") but without the thermal management system is chosen and the short-circuit current, open-circuit voltage, and power at different temperatures will be measured. The results of the BIPVT system are compared with this regular panel to see how much improvement in the parameters and ultimately in power is yielded. The maximum power point (MPP), which is a point on the I-V curve at which the maximum power output is achieved, is measured using an in-house I-V curve tracer. The corresponding voltage and current to this point, V_{MPP} and $I_{MPP,}$ respectively, are also determined.

In Figure 5(a), the designed solar panel with the temperature regulation system is shown. Nine thermocouples are used to collect the data during different times with and without the introduction of the water, as shown in Figure 5(b). Then, the results are mapped for almost 160 minutes showing how the panel's temperature changes over time before the hydronic system is on and after the cooling hydronic system is activated. The position of the thermocouples was chosen in a way to cover the whole area of the panel, but also to make sure the distribution of the double serpentine tubes is covered. In this way, the temperature profile of the panel can show how evenly the temperature is distributed after the flow of the water in the tubes begin. This is of significant importance since if there is a high-temperature difference between various points in the panel, not only the panel will not efficiently be cooled uniformly, but also the resulting thermal stress mismatch at different points will accumulate and cause microcracks over time. In addition to the nine thermocouples (T1 to T9) on the BIPVT panel, there are four more thermocouples to measure temperature associated with various aspects of the module. One is right at the outlet tube on the table to measure the temperature of the outlet water (T10). Since this thermocouple is exposed to the beams of the solar lamp as well and the output data

may be affected by the generated heat due to the lamp, another thermocouple is placed on the bottom shelf of the table to measure the outlet water temperature (T11).

The next thermocouple is exposed to the air and measures the ambient temperature (T12). This thermocouple is also placed on the bottom shelf to avoid any temperature biases from the light. Finally, the inlet water temperature from the building is measured by a thermocouple (T13) that is in the same room located on the bottom shelf before the water enters the particle filter. The average tap water temperature in New York City varies based on location and the season. This test was performed in the late springtime and the assumption was that the building's water temperature is about 25 °C. The test setup is shown in Figure 6. The BIPVT has been fully insulated from the sides and the bottom to avoid any heat loss while the system is running with and without water. This has been achieved by using Styrofoam insulator layers as well as soft sponges that are used for packing.

In order to capture data from the thermocouples, a data acquisition system (DAQ) from National Instruments was used (Figure 7). This DAQ has 16 channels which means it

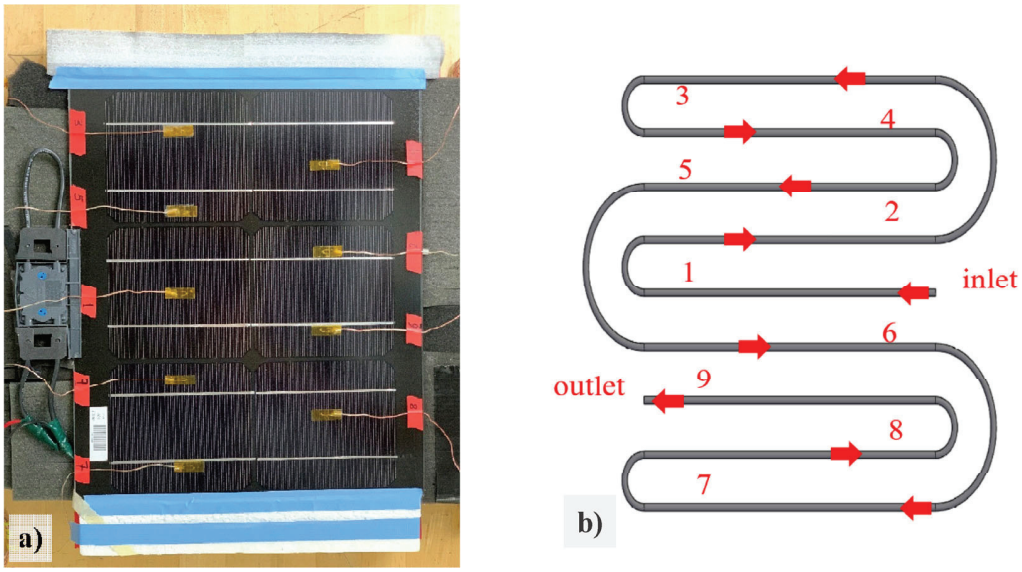

Fig. 5 (a) The prototype of the BIPVT design; (b) a schematic map of the position of the thermocouples on the panel with the tubing system

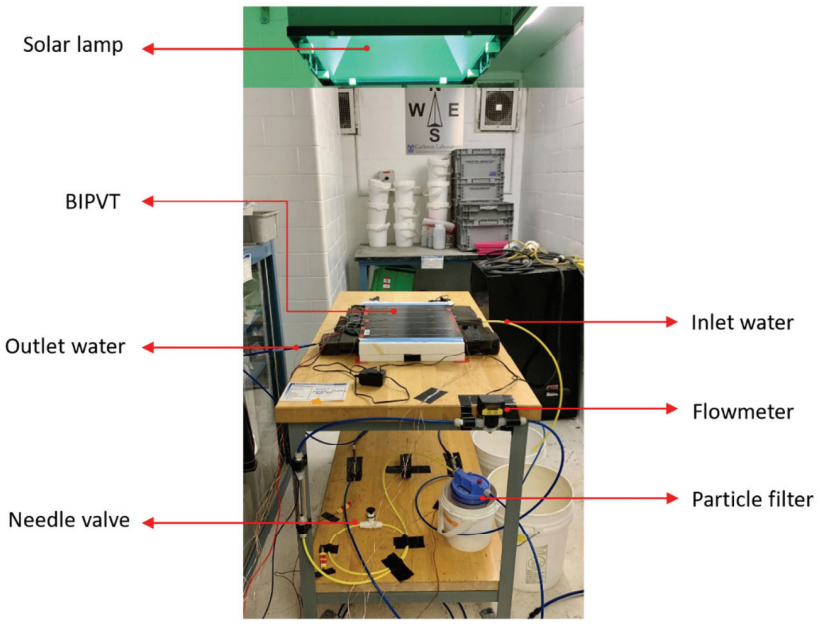

Fig. 6 Testing the solar panel under the simulated light with an intensity of 1000 W/m^2

can simultaneously be connected to 16 different sensors and support the generated data. The DAQ measures the output voltage signal and converts it into temperature. Then the software provided by the system called LabVIEW transforms the collected data into the .csv format. The data collection rate for this test was selected at 10 Hz to make sure the temperature variations are accurately recorded.

In order to measure the I-V curve, an in-house I-V curve tracer was used. Due to the small size of the solar module, it was not possible to use the available solar tracer in the lab. Thus, an accurate tracer for smaller modules was developed using the available design online, IV Swinger 2, which is a do-it-yourself (DIY) solar tracer for photovoltaic solar modules (Figure 8). Thanks to the open-source license, all the design components, and the software were provided online on the website (Satterlee 2019).

Just like any electronic instrument, the IV Swinger 2 has its own limitation. The main point of the design is the R1 and R2 resistors which limit the range of the measure open-circuit voltage (Voc). For our application, we chose

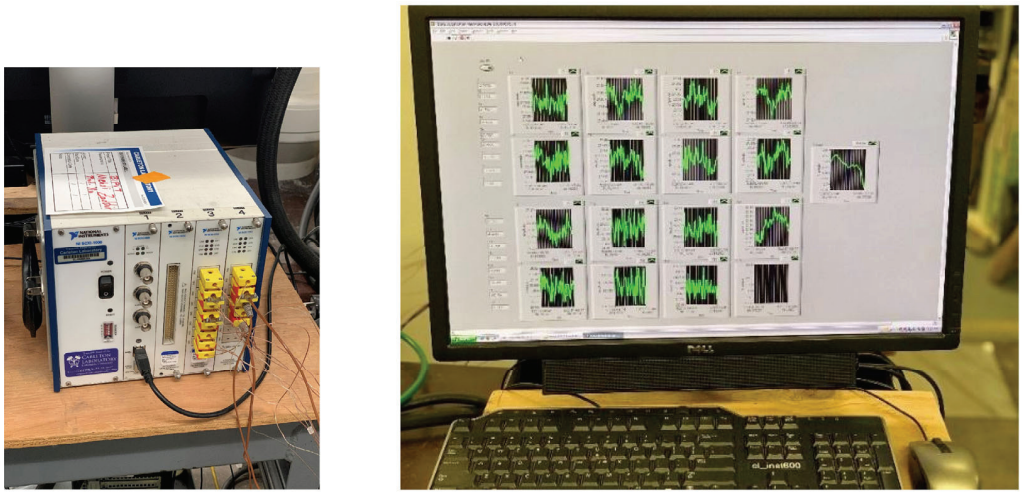

Fig. 7 A DAQ system is used to monitor the thermocouples data in real time

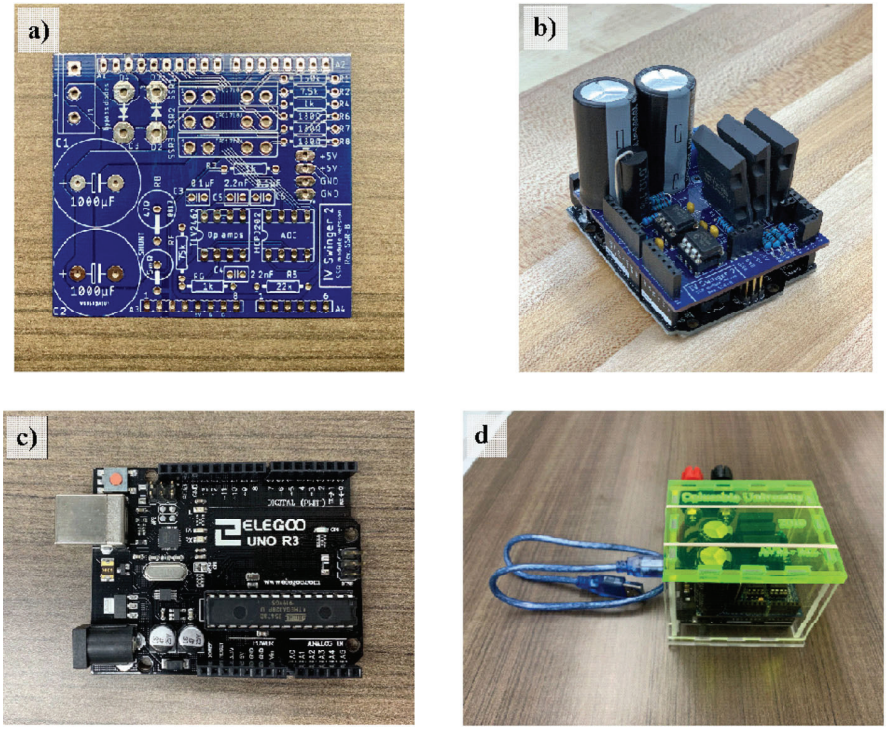

Fig. 8 (a) Printed circuit board (PCB) of IV Swinger 2; (b) assembled electrical components on the circuit board; (c) Arduino UNO R3 microcontroller; (d) finished product of the I-V tracer

R1 as 1 Ω (equivalent to the theoretical value of 0 Ω) and for R2, the resistance is 10 kΩ. The other limitation of the design is the short circuit current (Isc) that it can measure. Due to the internal resistance of the components, under 1 sun irradiation and by using Ohm's law, the first measured point of the current would be at 0.51 V, which is still fine for our application, since with temperature change, mainly the Voc changes over time, The Isc before the 0.51 V would be extrapolated by the provided software to calculate the output power. The data collection rate for the IV Swinger 2 can be looped so that the software can collect data automatically at a certain frequency. Here, the selected frequency rate is 1 Hz to make sure the changes in the I-V curve and the subsequent power are recorded accurately.

3.2 Numerical model setup

This paper conducts numerical simulation to evaluate the overall thermal performance of the system, which includes temperatures of the panel as well as inlet/outlet liquid. The model is primarily applied to examine the performance of the BIPVT system, and the results are later compared with the experiments. The results from the model are only applicable to the steady state condition that is achieved after t = 65 min following the test procedure flowchart (Figure 4). This is when the surface temperature of the panel and the outlet water stabilize while the water keeps circulating in the tubes. The steady state continues until the solar lamp is turned off (t = 95 min).

The numerical model was built based on the commercial software ANSYS 19.0. The governing equations for steady-state conjugate transfer can be found in reference (Nasrin et al. 2018; Misha et al. 2020; Salameh et al. 2021), which are not repeated here. To conduct the conjugate heat analysis, we employed the system-coupling mode that, (i) the steady-state thermal module uses the finite element method (FEM) to handle heat transfer of solids part; and (ii) the FLUENT module applies the finite volume method (FVM) to deal with heat transfer of liquid part. Since the numerical model uses two approaches to simulate the solid and liquid parts, the transferring data at the fluid-solid interface are coupled by the near-wall temperature, the temperature of the solids, and the heat transfer coefficient. During the simulation, ANSYS implements the average scheme to match the data transfer areas within a certain tolerance range. The iteration limiters can be adjusted according to accuracy, and we select $O(10^{-2})$ as the iteration target.

3.2.1 *Simulation geometry and material properties*

The simulation geometry includes working fluid, water tube, foamed aluminum substance, silicon PV cells, and the EVA (Figure 9).

The dimensions of the foamed aluminum box, water tube, and layers are shown below in Table 1.

The inner radius of the water tube is 1.6 mm, and the outer radius is 2.5 mm. The material of the water tube is aluminum with thermal conductivity of 237 W/(m·K). The cross-section of the working fluid is the same as the inner section of the water tube. For convenience in the experiments, water is selected for the working fluid, and its properties are listed below in Table 2.

3.2.2 *Boundary conditions*

As indicated in Figure 5(a) and Figure 6, the four side surfaces and the bottom surface of the aluminum box are covered with foams, and therefore they are considered

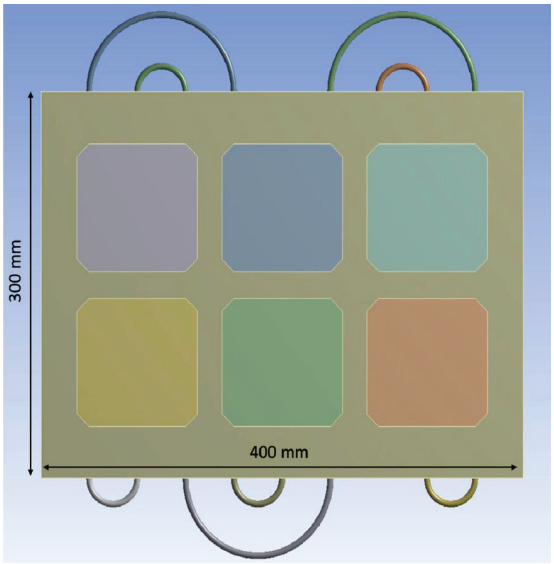

Fig. 9 Dimensions of simulation

Table 1 Dimensions and thermal conductivity of the different layers

Name of the layer	Thickness (mm)	Thermal conductivity (W/(m·K))
Silicon PV cells (6 pieces) and EVA layer	0.2	148 (silicon PV cells) & 0.35 (EVA)
Thermal paste	0.4	1.3
Glass	2.0	1.8
Foamed aluminum box	30	3.75
Aluminum water tube	0.9	237

Table 2 Material properties of the water

Material	Density (kg/m^3)	Dynamic viscosity (Pa·s)	Thermal conductivity (W/(m·K))
Water	1000	8.9×10^{-4}	0.59

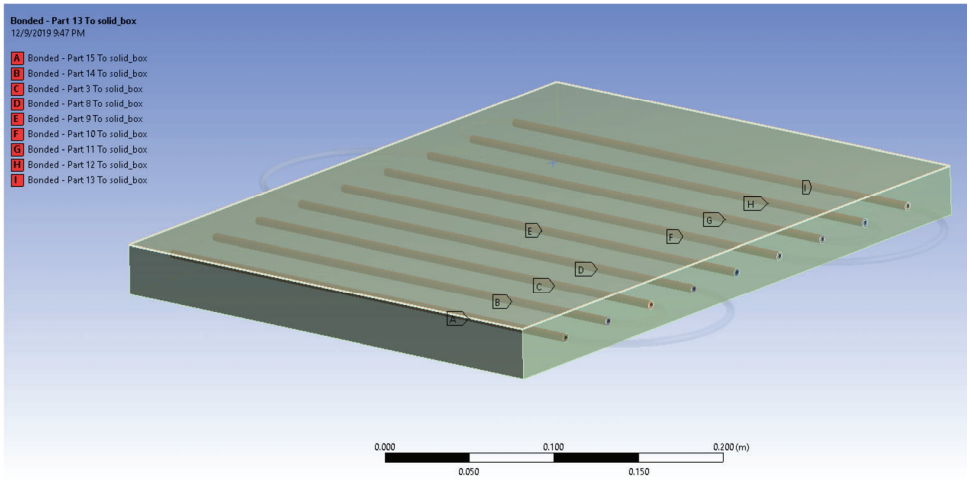

Fig. 10 Interaction definition area of the foamed aluminum box and water tubes

insulated boundary conditions in numerical simulation. The top surface of the box, specifically the glass layer, is subjected to the prescribed heat flux (light at the intensity of 1000 W/m^2) and air convection with the heat transfer coefficient h = 1.5 W/m^2 and reference ambient temperature 308.15 K. Due to the complexity of directly simulating foamed structures, an effective thermal conductivity (Paek et al. 2000; Dyga and Witczak 2012) has been used. Since the foamed aluminum box has been treated as one homogeneous matrix, an imperfect thermal contact between the water tubes and the foamed aluminum box is assumed. As indicated in Figure 10, the interaction area are defined in FEM, and the thermal contact conductance (TCC) is selected as 250 W/(m^2·K).

Following the experiment setup, the liquid is subjected to the following three initial/boundary conditions, (i) velocity inlet with the temperature at 295.45 K. (ii) zero pressure outlet. (iii) non-slip between the boundary layer and inner wall of the water tube. Given the flow rate of 100 and 200 ml/min, the Reynolds numbers (*Re*) are 372 and 744, respectively, which are below the turbulence range of 2000. Hence, in this work, the discussion is limited to the laminar flow.

3.2.3 *Domain discretization of solids and liquid*

Since both the FEM and FVM require domain discretization, it is natural to consider the employment of a close or similar element size to avoid high potential numerical errors during data transfer of system coupling. Compared to FEM, for guaranteed numerical stability, the CFL condition $v = \frac{\Delta t}{\Delta x} u$ (LeVeque 2002) is suggested to be controlled at less than 0.5 for transient analysis. However, this paper followed the ANSYS guide and adopts the density-based explicit solver for steady-state flow (Lynn 1995). The liquid domain is discretized through the sweeping method with an element size of 0.001 m, and the number of nodes and elements are 315,406 and 277,200, respectively.

As for the FEM part, two global element sizes are used to mitigate possible numerical errors in data transfer that, (i) all edges of the upper parts, including the aluminum box, solar modulus are applied with element size 0.002 m; and (ii) the water tubes are meshed with element size 0.001 m, which is the exact same one as the liquid. The number of nodes and elements is 2,684,201 and 772,381, respectively. Figure 11 shows the side view of the domain discretization of FEM mesh, which includes mesh on water tubes, layers of materials, and the aluminum box. The details of the iterative target and mesh irrelevance are elaborated in the Electronic Supplementary Material of the online version of this paper.

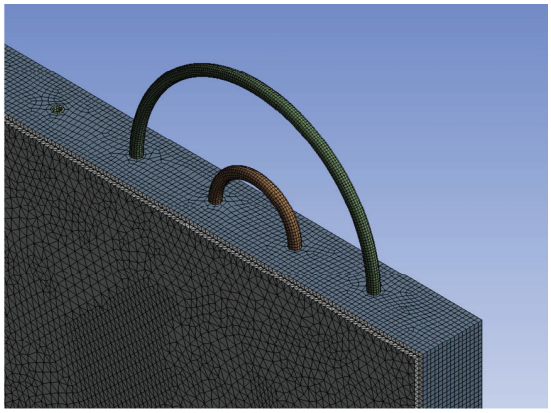

Fig. 11 Schematic plot of FEM mesh of the solid parts including water tubes, layers of materials, and the aluminum box

4 Results and discussion

The tested results from the thermocouples for the different water flow rates are shown in Figures 12(a)–(f). In the beginning, before starting the solar lamp, the panel is at room

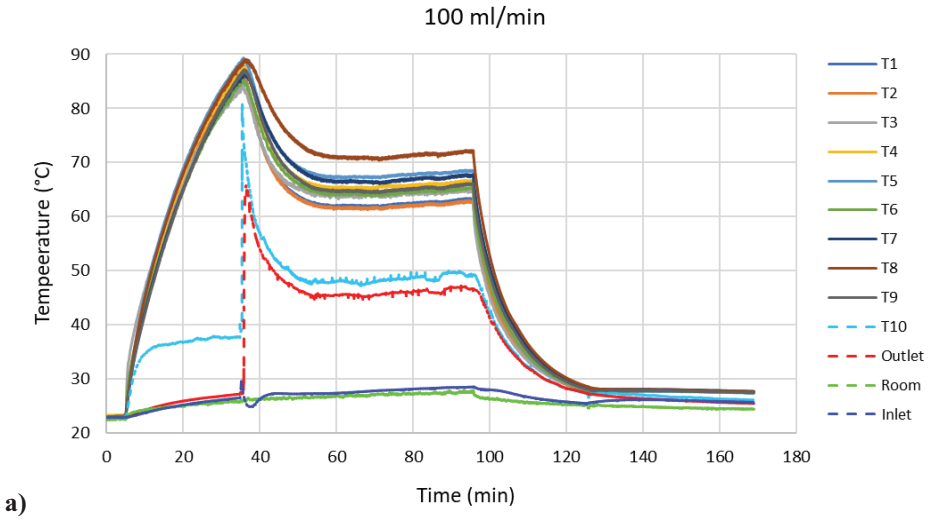

a)

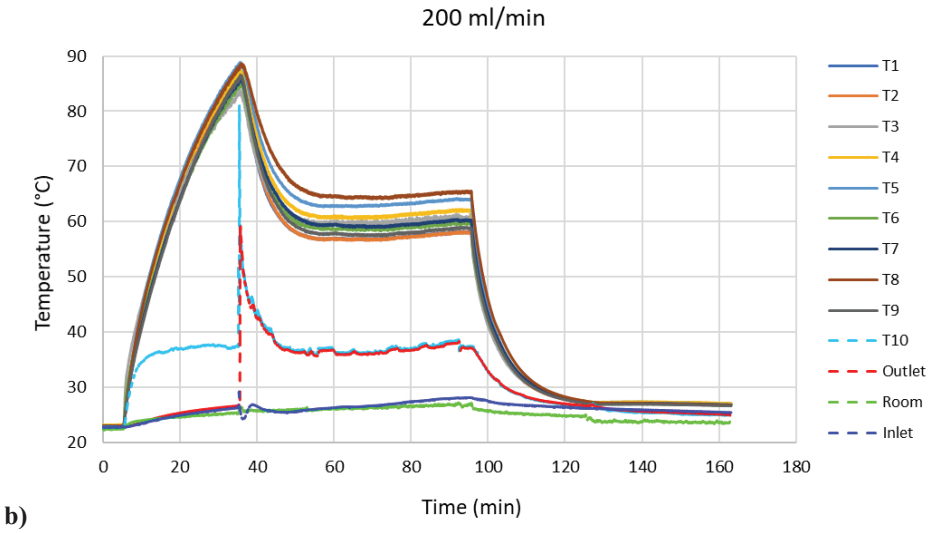

b)

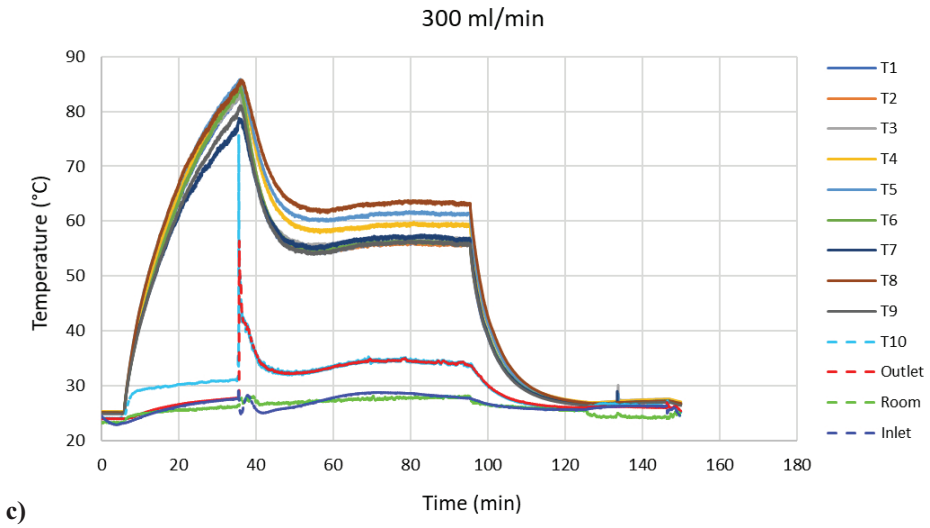

c)

Fig. 12 Monitored temperature of the thermocouples at: (a) 100, (b) 200, (c) 300, (d) 400, (e) 500, and (f) 600 ml/min flow rates before and after the introduction of the water

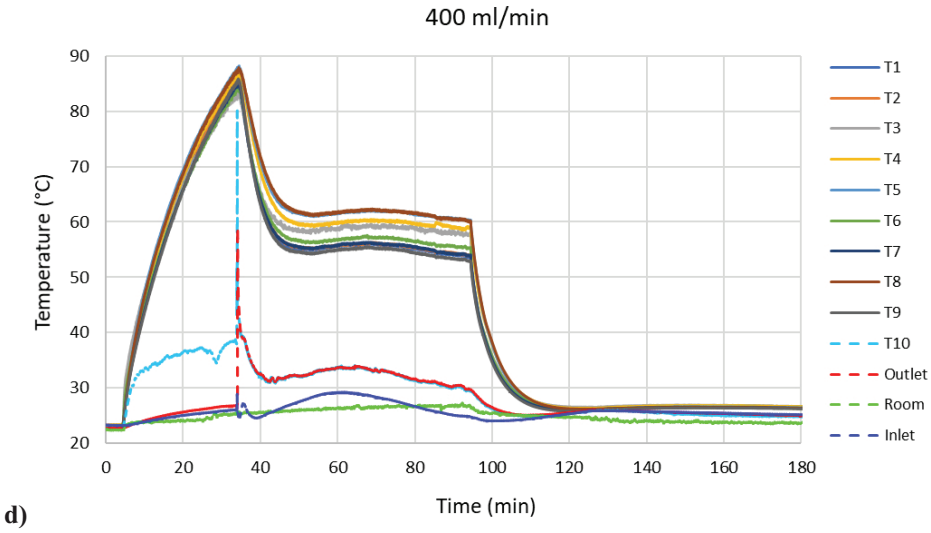

d)

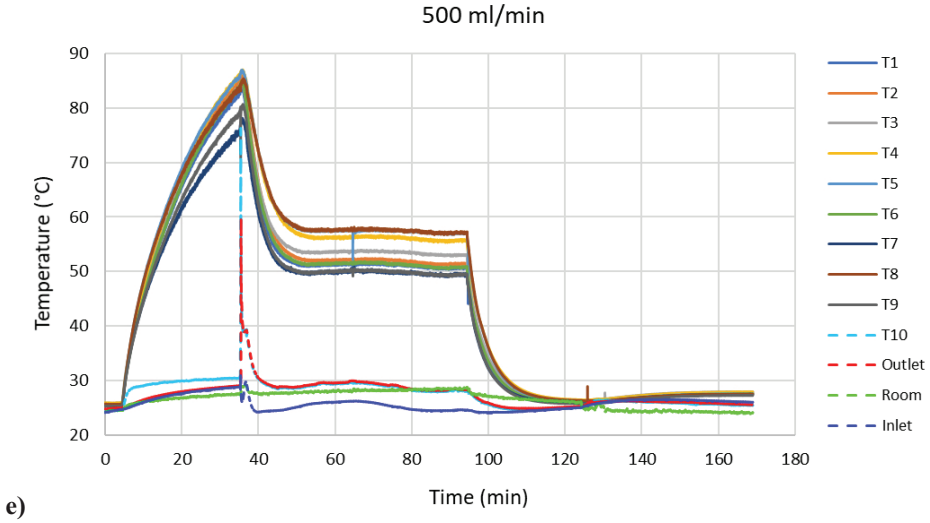

e)

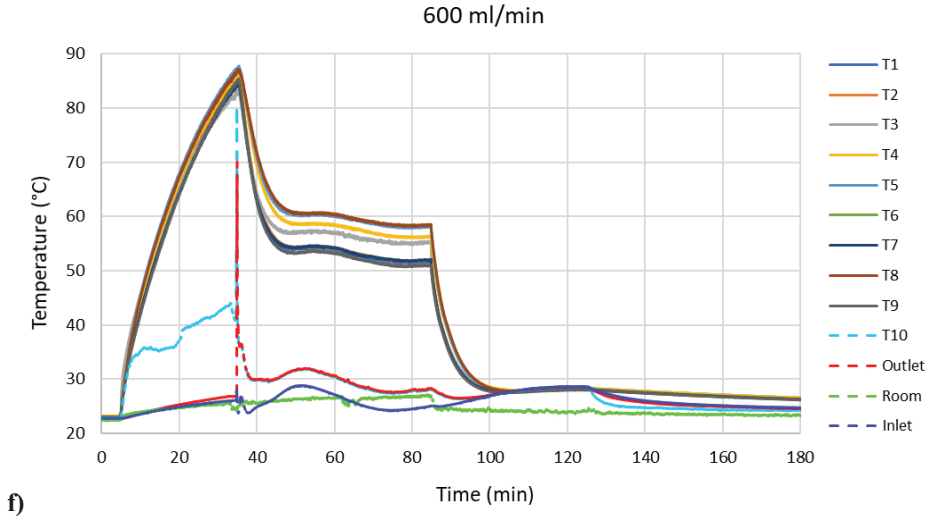

f)

Fig. 12 Monitored temperature of the thermocouples at: (a) 100, (b) 200, (c) 300, (d) 400, (e) 500, and (f) 600 ml/min flow rates before and after the introduction of the water (Continued)

temperature. Shortly after the lamp starts illuminating, the open-circuit voltage (Voc) reaches 3.60 V, and the short circuit current (Isc) 6.57 A. At this point, the maximum power point (MPP) is read at 14.89 W, which is somewhat similar to the original value that the manufacturer provided (14 W), and the V_{MPP} = 2.38 V and I_{MPP} = 6.26 A (Figure 13).

As time passes, the surface temperature of the panel increases reaching the highest point of almost 88 °C after 30 minutes. While there is a slight difference between the values read at different thermocouples placed on the panel (T1–T9), the peak is almost always recorded by T8 at 88 °C, which is near the outlet of the tube. At this point, the MPP voltage value has decreased to 1.85 V while the MPP current is at 5.79 A. We can see that the MPP power has significantly decreased from 14.89 W to 10.69 W due to the temperature increase. This is an almost 28.2% decrease in power.

When the water is introduced to the system, a sudden decay is observed in the temperature of the panel. We can see in Figure 12(a) that for a water flow of 100 ml/min, after about 30 min of water running in the system, the temperature of the panel stabilizes. Here, again T8 has the highest value of all the nine thermocouples being at 71 °C, while the other ones vary between 61 °C (T1 and T2) and 67 °C (T5). The temperatures stay stable until the solar lamp is turned off at t = 95 min, where we see a huge jump in the temperatures' values decreasing until they reach a stable point again at t = 135 min. It should be noted that following the defined procedure at the beginning of the experiment, at t = 125 min, the water inlet has been closed and since the panel's absorbing heat flux and the extracting heat had reached equilibrium at this point, it would be redundant to keep the water running any longer. After t = 135 min, all the nine thermocouples on the panel reach a steady temperature of 27 °C, and after t = 170 min, the DAQ system is turned off and the data acquisition stops. It should be noted that had we kept collecting the data after t = 170 min, we could see the temperature of the panel eventually reaching the starting point of 23 °C. However, due to the extensive amount of data that is generated by the sensors at a refresh rate of 10 Hz, it was decided to end the test after a stable temperature is observed on the panel.

As for the power output after the introduction of the water into the system, we can see that the power gradually starts to increase, and at the highest point, it reaches about 12.78 W, at which the V_{MPP} = 1.96 V and I_{MPP} = 6.52 A. This means that the hydronic system was able to revive the power by 19.5% from 10.69 W to 12.78 W. The MPP voltage and current have also accordingly improved from 1.85 V to 1.96 V and from 5.79 A to 6.52 A, respectively.

As for the temperature distribution of the double serpentine hydronic system, it can be seen that the readings from the thermocouples are all within an acceptable deviation of 8 °C difference after the water is introduced to the system. The values are in accordance with expectation, especially for T8 since this is where the heat is carried away to the outlet and the water should be at its highest point after circulating and collecting heat from the surface of the panel. It is speculated that with a different design, i.e., single serpentine or zig-zag, different values of temperature difference will be observed, which requires more design parametric analysis.

The other four thermocouples that are not located on the panel measure various properties related to this hydronic BIPVT panel. T10 located on the exit tube near the panel (Figure 6) and T11 (outlet water) underneath the table show the temperature of the exiting water from the panel. Before the water is circulated inside the tubes, T10 may be just showing the temperature of the tube exposed to the light and T11 the ambient temperature. When the water is opened at t = 35 min, a sharp spike is seen which is because the water starts running in the tubes and absorbing the heat to become warm. During the next 1 hour that the water keeps running in tubes, there is a temperature difference between the two thermocouples at a flow rate of 100 ml/min, while this is not observed at the other five flow rates, which could be because of the slow water flow.

For the other five flow rates, we see a similar trend in terms of the hydronic system effectively cooling the surface temperature of the BIPVT panel. However, there are differences in the intensity of temperature reduction as well as the outlet water temperature. In general, as expected, when the water flow is higher, the panel gets cooler and reaches a lower temperature. For example, at 100 ml/min, all nine thermocouples on the panel show a temperature above 60 °C, whereas when the flow rate is increased to 500 ml/min, the surface temperature of the panel reaches below 60 °C at all points.

As discussed, there is a correlation between the water flow rate and the cooling effect. One compromise here would be the outlet water temperature. Since a BIPVT panel can have a bifold purpose of cooling the solar panel and providing partially heated water for improving the efficiency of the hot water system for domestic building use. Therefore, if the flow rate of the inlet water is high, while the surface temperature of the panel gets cool sooner and the efficiency of the solar panel increases in addition to providing a larger volume of heated water per minute, the outlet water temperature would be lower and thus, resulting in the lower efficiency of the hot water system. Thus, in order to achieve the optimal flow rate of the system at which the highest power is achieved, and the temperature of the panel is efficiently reduced, several other analyses are needed. First, T4 is selected as the representative of the nine thermocouples. T4 data show to be somewhere in between

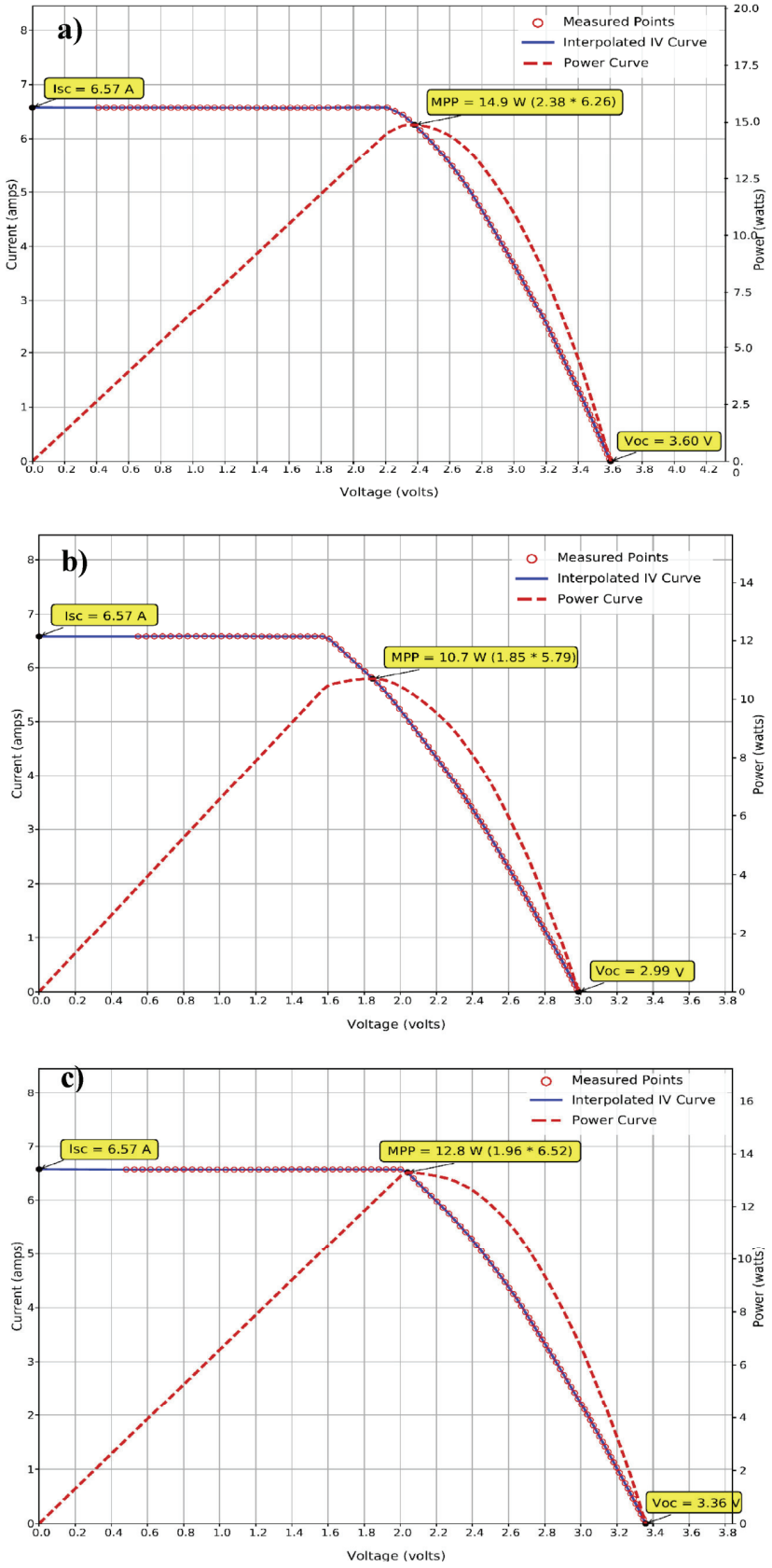

Fig. 13 Current vs. voltage and the output power in the BIPVT at (a) starting point (25 °C) without the water system; (b) after 30 min (88 °C) without the water system; (c) cooled state (65 °C) with 100 ml/min water flow rate

the highest and the lowest thresholds of the surface temperatures recorded. Also, T4 is not located on a corner of the panel and thus, can be a good selection.

We can see in Figure 14 that while at 100 ml/min, the largest difference is observed for T4, the data rest of the five flow rates are within a 5 °C difference. At t = 65 min, the highest value for T4 is read at 65.4 °C for a 100 ml/min flow rate. This value is 60.8 °C, 58.7 °C, 60.0 °C, 56.4 °C, and 57.6 °C for flow rates of 200, 300, 400, 500, and 600 ml/min, respectively. Despite the expectation, the higher flow rate does not necessarily result in a lower temperature. The extent to which cooling happens also depends on the time required for the aluminum tubes, water, and solar cells to exchange heat with each other and the surrounding environment to reach a steady state. Another noticeable observation is the fluctuation of temperature during the 1 h steady-state condition that the water is circulating, especially for a flow rate of 600 ml/min. It seems that the surface temperature has not reached a stable point.

In order to have a better judgment, the outlet water temperature has also been analyzed and shown in Figure 15. Here, the first thing that we notice is the large gap between the outlet water temperature at a flow rate of 100 ml/min versus the other five. We see that at t = 65 min, the exiting water temperature stabilizes at 45.4 °C for the flow rate of 100 ml/min. This value is much lower for the other flow rates being 36.3 °C, 34.1 °C, 33.8 °C, 29.9 °C, and 29.1 °C for 200, 300, 400, 500, and 600 ml/min, respectively.

The other notable observation is the temperature fluctuations for flow rates of 300, 400, 500, and 600 ml/min.

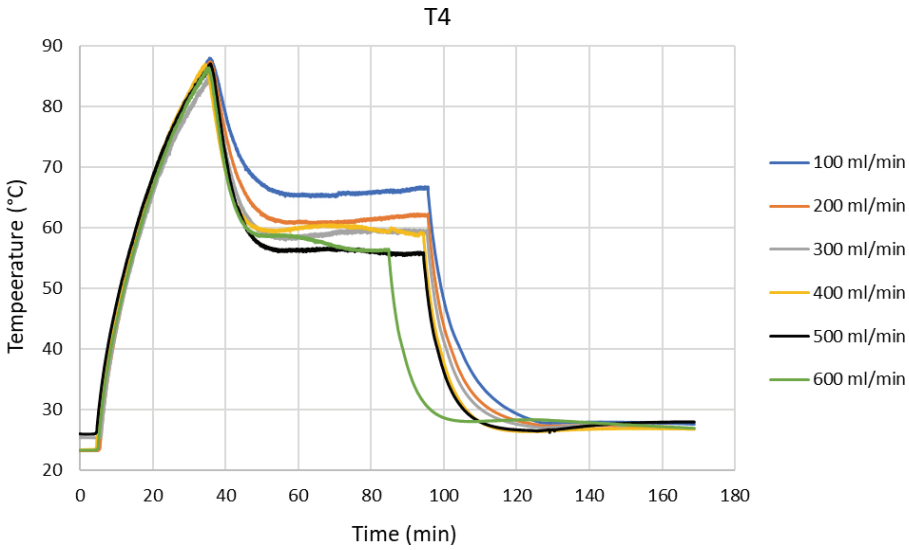

Fig. 14 T4 temperature vs. time for different flow rates

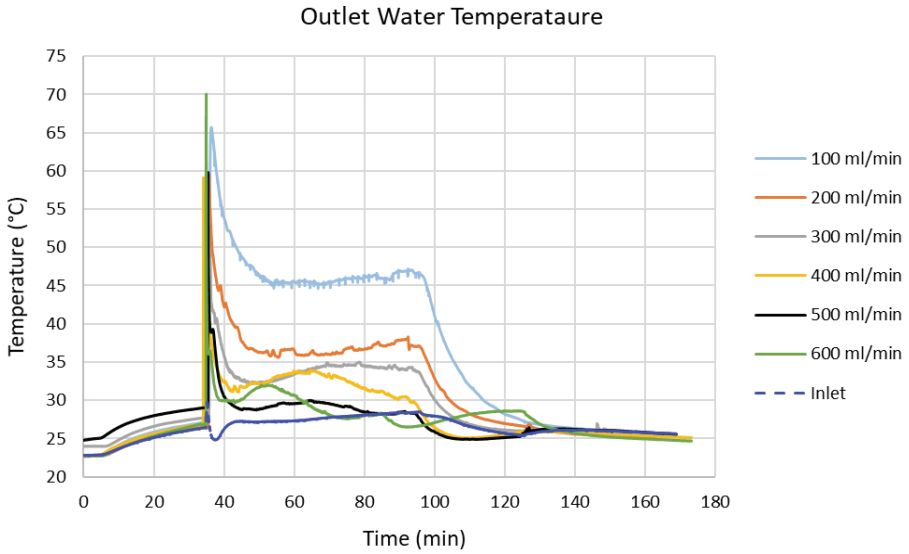

Fig. 15 Outlet water temperature (T11) vs. time for different water flow rates

One speculation could be that at flow rates higher than 200, the flow becomes turbulent and thus, causes fluctuations in the output temperature reading. To examine this guess, we can calculate the Reynolds number using Eq. (1):

$$Re = \frac{uL}{\nu} \tag{1}$$

where u is the flow speed, L is the dimension of the tube, and ν is the kinematic viscosity of the liquid. Based on the flowmeter unit (ml/min), we need to convert the unit to the form of mm^3/s in Eq. (2):

$$1\,\text{ml/min} = \frac{1}{60}\,\text{ml/s} = \frac{1000}{60}\,\text{mm}^3/\text{s} \tag{2}$$

Since we have:

$$L = D = 3.2\,\text{mm}, \qquad u = Q/A = Q \times \frac{1000/60}{\pi(1.6)^2}[\text{mm/s}] = 2.07233Q\,[\text{mm/s}],$$

and the kinematic viscosity $\nu = 1.787 \times 10^{-6}\ \text{m}^2/\text{s}$. Here, Q is the quantum as in the flowmeter. Thus, the Reynolds number is obtained as shown in Eq. (3):

$$Re(Q) = \frac{uL}{\nu} = \frac{2.07233 \times Q \times 10^{-3} \times 3.2 \times 10^{-3}}{1.787 \times 10^{-6}} = 3.7109Q \tag{3}$$

When the Reynolds number is larger than 2100, it will be considered as a transition status from laminar to turbulent flow. Therefore, when the flow quantum $Q \le 565$ or to be safe $Q \le 500$, we can still consider it laminar.

Having the turbulent hypothesis is voided and by looking closer at the inlet water temperature at each flow rate, we see a fluctuation in the inlet temperature in $Q \ge 300$ ml/min. Especially since the patterns of hills and valleys for increases and decreases of the inlet and outlet temperature match each other while considering the temperature shift due to the BIPVT system. Therefore, the reason we see such fluctuations in the outlet water temperature could be the instability of the building's tap water temperature.

The other factor determining the optimal flow rate is the harvesting power from the solar module and the efficiency of each flow compared with the other ones in reviving the lost power due to the heat. The output power versus time is shown in Figure 16. Here, we can clearly see the decay in power as the module's surface temperature increases over time. At t = 35 min, the water valve is opened and the hydronic system is activated. We can see the increase in the power as the water keeps circulating in the tubes until about t = 65 min. When the solar light is turned off at t = 95 min, the data collection is stopped automatically.

By comparing the initial power values with the point at which maximum power loss has occurred, we see a reduction of power from about 14.89 W to 10.69 W due to the temperature increase. This is an almost 28.2% decrease in power. However, once, the hydronic system reaches a stable steady point, we can see that the power is increased to 12.68 W, 13.32 W, 13.05 W, 13.66 W, 13.54 W, and 13.92 W for flow rates of 100, 200, 300, 400, 500, and 600 ml/min, respectively, which means an increase of 18.6%, 24.6%, 22.07%, 27.7%, 21.0% and 30.2% of the power values.

By and large, considering the cooling effect of the surface temperature of the solar module, the outlet water temperature, and the resulting power output increase due to the hydronic system, it seems that choosing the flow rate of 200 ml/min would result in an overall effective BIPVT panel with the optimum power and hot water generated. Of course, this value is selected based on the current design and regarding the limited accessible measurement that was performed.

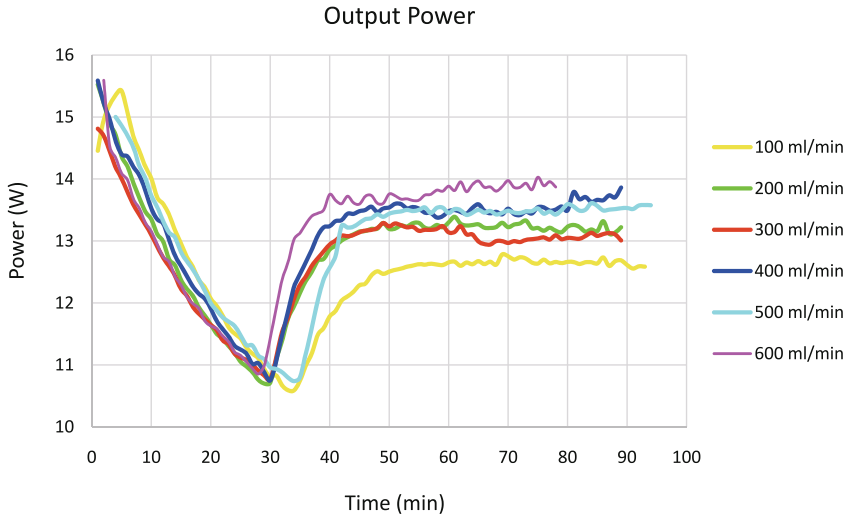

Fig. 16 Power vs. time for different water flow rates

5 Comparison between experiments and steady-state simulation

Here, two cases have been studied following the experimental section. One with a water flow rate of 100 ml/min and the other with a water flow rate of 200 ml/min. In the performance testing, Q = 100 ml/min showed to have the highest water output temperature, whereas Q = 200 ml/min overall showed to be the optimal flow to achieve a high cooling effect and subsequent increase in the outlet power while also reaching a partially warm water output.

The results for the flow rate of 100 ml/min are shown in Figure 17 and Figure 18. In Figure 17 only the temperature of the top surface of the panel is shown. The inlet is marked with a green arrow and the outlet with a red arrow. We can see that for T1, the temperature is at 60.27 °C when the panel reaches a steady-state condition. This is quite similar to the recorded temperature for T1 during the experiment as it showed to be 61.92 °C at t = 65 min when the panel

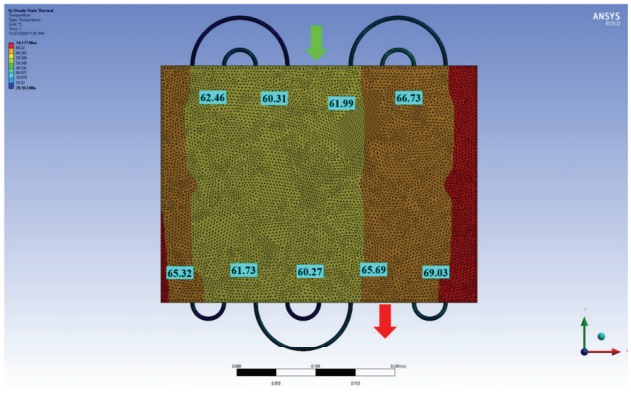

Fig. 17 Temperature distribution of the top surface at the steady state with a flow rate of 100 ml/min

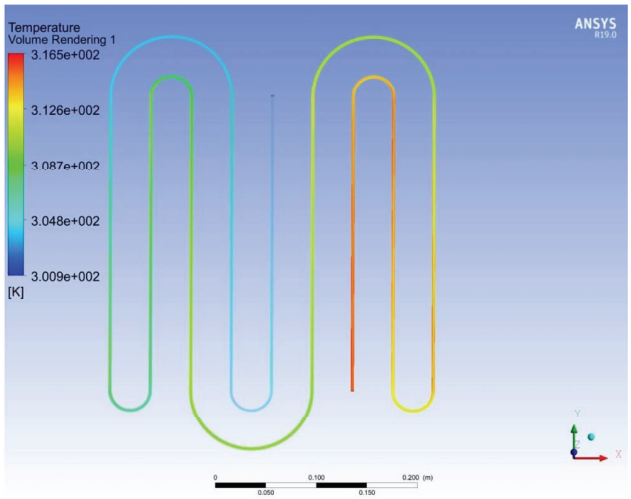

Fig. 18 Temperature distribution of the water path at the steady state with flow rate at 100 ml/min

reached temperature equilibrium. As the water is exposed to the collected heat from the solar cells transferred by the conductive carbon adhesive tape between the solar module and the aluminum foamed layer, the temperature of the water increases.

Let us look at another example in the corner of the panel, for example, the location of T3. The experiment showed a temperature of 63.82 °C for T3 at t = 65 min, whereas here in the simulation result, we see a temperature of 65.32 °C. This slight discrepancy could be due to the simulation design and the incorporated parameters for the different layers of the panel. However, by looking at the experimental data of T3 at t = 95 min, shortly before the solar lamp is turned off, we see that the temperature reaches 64.70 °C which is much closer to what the simulation data showed. Finally, looking at the T9 which is located at the exit of the tubing system, we see that the data from the simulation shows a temperature of 65.69 °C at the equilibrium, while from the experiment, this reading is 64.86 °C at t = 65 min. Once again, the results from the experiment and the simulation quite match and show the accuracy of the simulation prediction. As for the water temperature, we can see the outlet water temperature reaches 43.35 °C when exiting the panel, close to what was measured in the experiment with the value of 45.4 °C.

As for the case with Q = 200 ml/min, the results are shown in Figure 19 and Figure 20. For the location of T1 at the entrance of the hydronic tubing system, the simulation result shows a reading of 57.07 °C, and the experiments showed 56.88 °C. For T3, we can see in Figure 19 that it shows a temperature of 60.86 °C, whereas the experimental reading is 59.46 °C at t = 65 min (steady state condition) and 60.49 °C for t = 95 min. Finally, for T9 located at the outlet point, the simulation shows 60.42 °C while the experimental temperature is 58.76 °C, a slightly larger difference compared with the other cases, but still within the acceptable range.

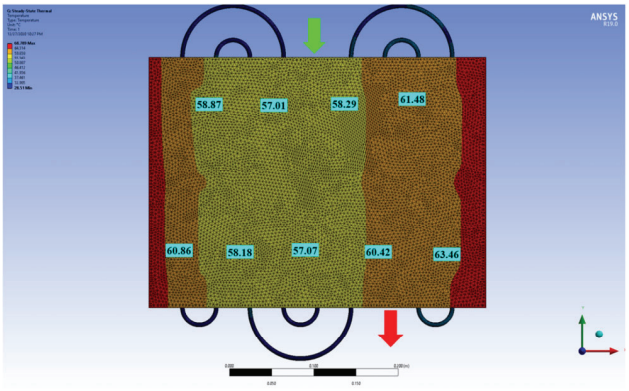

Fig. 19 Temperature distribution of the top surface at the steady state with a flow rate of 200 ml/min

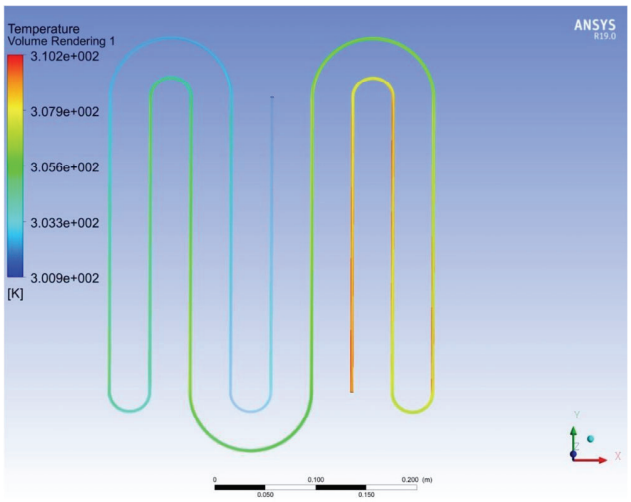

Fig. 20 Temperature distribution of the water path at the steady state with a flow rate of 200 ml/min

Overall, the results quite well fall within the acquired data from the experiment, validating that the model can be used to predict future cases and more complicated designs. For example, one downside of the current double serpentine hydronic design is the thermal mismatch between the center and sides of the panel, as confirmed by both the experimental and the simulation results. This in the long run could result in stress accumulation and accelerate the degradation or even cracking of the solar cells. Therefore, it is important to modify the design in future iterations.

6 Conclusions

In this work, a novel design for a building integrated photovoltaic thermal (BIPVT) system was introduced and its performance was tested using experiments and computer simulations. For experiments, six flow rates of 100 to 600 ml/min with an increment of 100 were selected and the experiments were run for over 160 minutes in total so that the system reaches a stable point for readings of temperatures and power. An I-V tracing system was developed to capture the changes in current and voltage and the subsequent power due to the implementation of the cooling system. For simulations, the finite element method and finite volume method were used to simulate the temperature of the panel and the output liquid after the steady state condition is achieved after t = 65 min. The results show that the hydronic system effectively reduced the surface temperature of the panel from almost 88 °C to as low as 55 °C. Although there was a difference in the measured temperatures by the nine thermocouples, the deviation was within 8 °C. The hydronic design revived the lost power by 30.2% while varying for different flow rates. The temperature of the outlet water depends on the incoming water flow rate with the highest temperature of 45.4 °C achieved at a flow rate of 100 ml/min, and the lowest temperature of 29.1 °C at 600 ml/min. The results from the simulations at the steady-state conditions are in good agreement with the experiment as well with a discrepancy of less than ±3.0% for the surface temperature readings. Overall, the flow rate of 200 ml/min could be selected as the optimal flow rate to achieve both the balance of the cooling effect and the acceptable output water temperature, although further analysis can be done to find the optimum rate considering the collected heat per area and the amount of energy saving.

Electronic Supplementary Material (ESM): the supplementary material is available in the online version of this article at https://doi.org/10.1007/s12273-023-1027-z.

Acknowledgements

This work is sponsored by the National Science Foundation IIP #1941244, CMMI #1762891 and U.S. Department of Agriculture NIFA #2021-67021-34201, whose support is gratefully acknowledged.

Declaration of competing interest

The authors have no competing interests to declare that are relevant to the content of this article.

Author contribution statement

M. Zadshir: material preparation, data curation, visualization, writing—original draft; C. Wu: simulation, data curation, writing—review & editing; X. Yu: material preparation, data curation; H. Yin: conceptualization, resource, supervision, writing—review & editing.

References

Ananthachar V (2008). Current and next generation solar cell market outlook. In: Proceedings of ISES World Congress.

Bejan A (2013). Convection Heat Transfer, 4th edn. Hoboken, NJ, USA: John Wiley & Sons.

Chen F, Yin H (2016). Fabrication and laboratory-based performance testing of a building-integrated photovoltaic-thermal roofing panel. *Applied Energy*, 177: 271–284.

Chen F, Pao F, YinH (2018). Advanced building integrated photovoltaic/thermal technologies. In: Letcher TM, Fthenakis VM (eds), A Comprehensive Guide to Solar Energy Systems. Amsterdam: Elsevier.

De la Torre J, Bremond G, Lemiti M, et al. (2006). Silicon nanostructured layers for improvement of silicon solar cells' efficiency: A promising perspective. *Materials Science and Engineering*: *C*, 26: 427–430.

Dyga R, Witczak S (2012). Investigation of effective thermal conductivity aluminum foams. *Procedia Engineering*, 42: 1088–1099.

Fraas LM (2014). History of solar cell development. In: Low-Cost Solar Electric Power. Cham, Switzerland: Springer.

Fthenakis VM, Lynn PA (2018). Electricity from Sunlight: Photovoltaic-Systems Integration and Sustainability. Hoboken, NJ, USA: John Wiley & Sons.

Ghani F, Duke M, Carson JK (2012). Estimation of photovoltaic conversion efficiency of a building integrated photovoltaic/thermal (BIPV/T) collector array using an artificial neural network. *Solar Energy*, 86: 3378–3387.

Ghosh K (2017). Status and Technology of Present Day Solar Cells. In: Proceedings of the 3rd International Conference, OPTRONIX 2016.

Lamnatou C, Mondol JD, Chemisana D, et al. (2015). Modelling and simulation of Building-Integrated solar thermal systems: behaviour of the coupled building/system configuration. *Renewable and Sustainable Energy Reviews*, 48: 178–191.

LeVeque RJ (2002). Finite Volume Methods for Hyperbolic Problems. Cambridge, UK: Cambridge University Press.

Lin Q, Zhang Y, Van Mieghem A, et al. (2020). Design and experiment of a sun-powered smart building envelope with automatic control. *Energy and Buildings*, 223: 110173.

Lynn JF (1995). Multigrid solution of the Euler equations with local preconditioning. PhD Thesis, University of Michigan, Ann Arbor, USA.

Misha S, Abdullah AL, Tamaldin N, et al. (2020). Simulation CFD and experimental investigation of PVT water system under natural Malaysian weather conditions. *Energy Reports*, 6: 28–44.

Nasrin R, Hasanuzzaman M, Rahim NA (2018). Effect of high irradiation and cooling on power, energy and performance of a PVT system. *Renewable Energy*, 116: 552–569.

Natarajan SK, Mallick TK, Katz M, et al. (2011). Numerical investigations of solar cell temperature for photovoltaic concentrator system with and without passive cooling arrangements. *International Journal of Thermal Sciences*, 50: 2514–2521.

Paek JW, Kang BH, Kim SY, et al. (2000). Effective thermal conductivity and permeability of aluminum foam materials[1]. *International Journal of Thermophysics*, 21: 453–464.

Salameh T, Tawalbeh M, Juaidi A, et al. (2021). A novel three-dimensional numerical model for PV/T water system in hot climate region. *Renewable Energy*, 164: 1320–1333.

Satterlee C (2019). IV Swinger 2. Available at https://www.instructables.com/IV-Swinger-2-a-50-IV-Curve-Tracer/

Ushasree P, Bora B (2019). Silicon solar cells. In: Gibson EA (ed), Solar Energy Capture Materials. London: The Royal Society of Chemistry.

Yang D, Yin H (2011). Energy conversion efficiency of a novel hybrid solar system for photovoltaic, thermoelectric, and heat utilization. *IEEE Transactions on Energy Conversion*, 26: 662–670.

Yang DJ, Yuan ZF, Lee PH, et al. (2012). Simulation and experimental validation of heat transfer in a novel hybrid solar panel. *International Journal of Heat and Mass Transfer*, 55: 1076–1082.

Yin HM, Yang DJ, Kelly G, et al. (2013). Design and performance of a novel building integrated PV/thermal system for energy efficiency of buildings. *Solar Energy*, 87: 184–195.

Zadshir M, Wu C (2019). Design and development of a hydronic system for temperature regulation and heat harvesting in a building integrated photovoltaic thermal panel. In: Proceedings Energy Harvesting from Infrastructure and Ocean Systems (EHIOS).

Zhang Y, Lin Q, Van Mieghem AE, et al. (2019). Solar window blinds with passive cooling coating and smart controllers. In: Proceedings Energy Harvesting from Infrastructure and Ocean Systems (EHIOS).

Zhang L, Lin Q, Chen F, et al. (2020). Micromechanical modeling and experimental characterization for the elastoplastic behavior of a functionally graded material. *International Journal of Solids and Structures*, 206: 370–382.

Zhang Y, Lin Q, YinH (2021). Thermoelastic modeling of layered composites considering bending and shearing effects. *Journal of Engineering Mechanics*, 147: 04021034.